Hős, C. J., Champneys, A. R., Paul, K., & McNeely, M. (2016). Dynamic behaviour of direct spring loaded pressure relief valves: III valves in liquid service. *Journal of Loss Prevention in the Process Industries*, *43*, 1-9. https://doi.org/10.1016/j.jlp.2016.03.030

University of Bristol - Explore Bristol Research
General rights

Dynamic behaviour of direct spring loaded pressure relief valves: III valves in liquid service [☆]

C.J. Hős[a], A.R. Champneys[b], K. Paul[c], M. McNeely[c]

[a]*Department of Hydrodynamic Systems, Budapest University of Technology and Economics, 1111 Budapest, Műegyetem rkp. 3. Budapest, Hungary*
[b]*Department of Engineering Mathematics, University of Bristol, Queen's Building Bristol BS8 1TR, UK*
[c]*Pentair Valves and Controls, 3950 Greenbriar Drive, Stafford, TX 77477, USA*

Abstract

Previous studies into direct-spring pressure relief valves connected to a tank via a straight pipe are adapted to take account of liquid sonic velocity. Good agreement is found between new experimental data and simulations of a coupled fluid-structure mathematical model. Upon increasing feed mass flow rate, there is a critical pipe length above which a quarter-wave instability occurs. The dependency is shown to be well approximated by a simple analytical formula derived from a reduced-order model. Liquid service valves are found to be stable for longer inlet pipes than for the gas case. However, the instabilities when they do occur are more violent and the valve is found to jump straight into chatter, in which it impacts repeatedly with its seat. Flutter-type oscillations are never observed. These observations are explained by finding that the quarter-wave Hopf bifurcation is subcritical. Water hammer effects can also be observed, which result in excessive overpressure values during chatter. In addition a new, Helmholtz-like instability — not encountered in gas service — is identified for short pipes with small reservoir volumes. This can also be predicted analytically and is shown to explain a valve-only instability found in previous work that incorporated significant mechanical damping.

Keywords: pressure-relief valve, reduced order modeling, instability, quarter-wave, Hopf bifurcation, water hammer

---

[☆]Short title: Dynamics of liquid pressure relief valves

Contents

1. Introduction

This paper continues the previous work by the present authors in Hős et al. (2014, 2015) on practical considerations of mechanisms of instability in direct spring operated pressure relief valves (PRVs). Here we specifically consider valves in liquid, rather than gas, service. Current guidelines (such as the API RP520) for avoiding valve flutter and chatter in both gas and liquid cases, refer to the need to avoid inlet pressure losses due to pipe friction of more than 3% of the set pressure of the valve. The logic of this criterion is to avoid so-called rapid cycling motion, in which pressure loss causes the valve to shut prematurely, only to open again soon afterwards. The believed sufficiency of this criterion can be traced back to work of Frommann and Friedel (1998) who studied valve vibrations in pneumatic systems both numerically and experimentally. However, as shown in Hős et al. (2014) for gas and in Figs. 3 and 4 below for liquids, this criterion does not seem to capture the correct parameter trends especially for low mass flow rates.

Instead, in Hős et al. (2015) we found an accurate stability criterion which we tested against experimental results for three different commercially available gas service PRVs. The key is to recognize that the fundamental instability causing valve flutter is a flow-induced *Hopf bifurcation* caused by an interplay between the valve natural dynamics and the fundamental *quarter-wave* acoustic vibration mode in the pipe. Effectively, the valve can supply *negative damping* to the acoustic mode; which is an explanation that does not rely on there being any internal resonance. The trend for this instability was found to be such that for each mass flow rate up to full capacity, there is a critical inlet pipe length beyond which the valve is unstable, with an approximately square-root dependence between the critical pipe length and the mass flow rate. For a yet longer pipe, the limit-cycle flutter behavior will undergo a transition into large-amplitude chatter motion in which the valve impacts with its seat. Moreover, through reduced-order modelling, in Hős et al. (2015) we were able to produce a close analytical approximation to this curve which depends only a few pipe and valve parameters. In addition, specific features of the valve geometry can cause static jumps, or *fold bifurcations*, but these do not necessarily lead to flutter and shall not be considered in the present work.

The purpose of this paper is to extend that work to deal with the case of liquids. The paper Hős et al. (2014) contains a comprehensive literature review on instabilities of pressure relief valves, focusing mostly on the case

of gas pipes. We give here only additional references relevant to the liquid case.

Licsko et al. (2009) assembled a simple system of ordinary differential equations describing the motion of a valve connected to a hypothetical hydraulic chamber. They performed linear and non-linear stability analyses and found parameter ranges where flutter-induced limit cycles turn into chattering motion through *grazing bifurcations*. At the opposite end of the spectrum of computational complexity, Song et al. (2010), produced a 3D CFD model with deforming mesh for investigating the precise flow physics of transient valve motion at instability. Moussou et al. (2010) investigated both static and dynamic instabilities through a mixture of analytical calculations, CFD and experiments. They also introduced the concept of what is referred to in our work as the *effective area* of the valve at a given lift (called the *equivalent surface* by Moussou et al. (2010)) and investigated the appearing limit cycle. Similar concepts were developed by Viel and Imagine (2011) who studied stability with the help of Nyquist plots, and by Beune et al. (2012) who calculated flow force versus displacement using more computationally efficient 2D CFD. Further developments in full CFD simulations for liquid service PRVs have been undertaken by various authors showing just how complex the flow field can be, depending on the valve geometry and turbulence model adopted: see Dossena et al. (2013); Qian et al. (2014); Song et al. (2014, 2013); Wu et al. (2015).

Bazsó and Hős (2012) investigated the need for unsteady CFD for predicting the point of onset of the instability by, comparing 2D simulations with full 3D deforming mesh computations for a simple conical valve body. They found that both were able to capture the same point of instability, even reaching agreement on the nature of the appearing limit cycle, sufficiently close to the instability point. These predictions were also found to match well with experiments. Furthermore, recent work by Erdődi and Hős uses 2D CFD computations with both stationary and moving meshes to justify the use of simple effective-area-versus-lift curves and single discharge coefficients. Those results appear to justify the use of reduced-order modelling for instability prediction, even for liquids where the unstable motions tend to be much more violent than for gas flows. This violence is due to the significant additional momentum in the fluid, which would otherwise be dissipated in compressible fluids.

Such reduced-order models were studied in a series of papers: Hős and Champneys (2012); Bazsó et al. (2015, 2014). These works produce a simple

4

dimensionless models of liquid service PRVs without fitting parameters to a particular set of test valves. Another form of Hopf bifurcation also leading to flutter and chatter was discovered, referred to as a *valve only* or *Helmholtz-like* instability. This instability was found to occurs for finite mass-flow rates even in the limit that the pipe length tends to zero. It is of important to note though that that those studies assumed significant mechanical valve damping, which is unrealistic for commercial valves.

The rest of this paper shall follow a similar approach to that in Hős et al. (2014) and Hős et al. (2015). In Sec. 2 we present the results of dedicated tests of valves in liquid service connected to a reservoir via a straight pipe of variable length to document cases that lead to instability, and the nature of the instabilities observed. Then, Sec. 3 presents our previous mathematical models and their modification to the problem at hand. We also present a new analysis on the cause of the Helmholtz-like instability. Sec. 4 presents numerical simulations of the model, along with parameter studies and comparison with both experiments and the analytical predictions of the quarter-wave and Helmholtz-like instabilities. Finally, Sec. 5 draws conclusions and discusses practical significance of the work.

2. Experimental results

2.1. Test procedure

A series of tests were conducted in the Pentair test facility using the rig depicted in Fig. 1 in which pressurized water is connected to a valve via a straight inlet pipe. The length of the pipe can be varied from 0 to 12 feet by carefully fitting together pipe segments of different lengths. The pressure in the feeder tank is closely controlled by means of a supply from a larger tank whose pressure can be increased via a drive of nitrogen gas. A nitrogen vent can be opened in order to reduce the tank pressure. Two different industry standard valve types were used, a 2J3 and a 1E2. It should be stressed that neither of these valves were fitted with specific liquid trims. The gas trim used was identical to that used for the gas-service tests Hős et al. (2014), so as to enable a direct comparison.

A total of over fifty tests were performed for different pipe lengths and different desired mass flow rates. In each run, the drive pressure (labelled PD in Fig. 1) was slowly ramped up to a fixed value that enables a mass flow rate of the desired percentage of the valve's capacity. The drive pressure was held steady for about 20 seconds before the nitrogen valve was opened and the
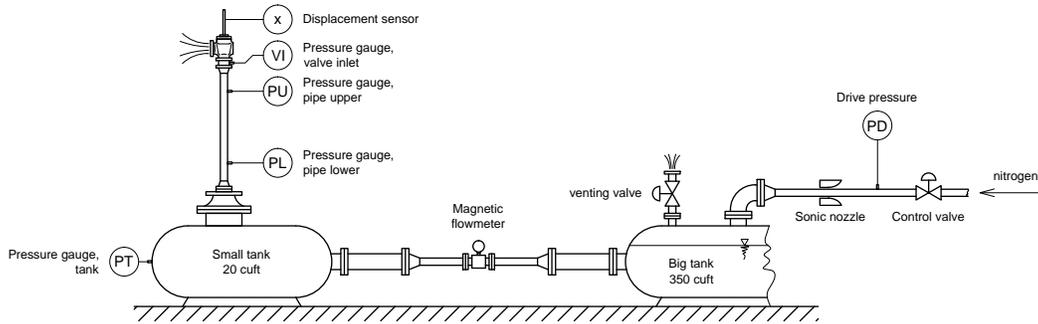
Figure 1: The liquid test rig. Each abbreviation inside a circle depicts a point at which measurements were taken. See text for details.

pressure ramped down. All tests were performed with a nominal opening set pressure of 120 psig (8.27 bar). The actual opening pressure was measured from the data at the valve inlet (labelled VI), at the instant when the lift first reaches 1% of its maximum possible lift. This pressure was typically found to be within a few percent of the nominal set pressure. Blowdown pressure was nominally set to be 114 psig (7.86 bar, or 5% of set pressure), but was similarly measured as the VI pressure at which the lift falls beneath 1% after the valve has been open for at least 1 second. However, as can be seen from the example time traces in Fig. 2 below, the measurement of blowdown in particular was found to be problematic due to the noisy nature of the pressure response in the pipe.

The capacity (flow rate at full lift and 10% above set pressure) of the two valves was nominally 400 USgpm (25.23 kg/s) for the 2J3 and 70 USgpm (4.41 kg/s) for the 1E2 valve. These values and measurements of the rate of pressure loss at capacity allowed us to determine the discharge coefficient C_d corresponding to the *curtain area* $D_{bore}\pi x_{valve}$ of each valve. We thus obtained C_d-values of 0.36 and 0.32 respectively for the 2J3 and the 1E2 valves.

Accurate measurement of sonic velocity is important for matching with simulations, because it plays a crucial role in the dynamic interaction between the pipe and the valve. The standard value for fresh water in an infinitely rigid pipe or reservoir would be about 4700ft/s (1430m/s) but both pipe wall elasticity and air content within the water reduce this value in practice. We measured sonic velocity using the following procedure. Upon valve closing, pressure waves are generated in the pipe, which are then reflected back from

6

the reservoir end of the pipe. The time needed for one full cycle is

$$T_{\text{pipe}} = \frac{2L}{a}, \tag{1}$$

with a being the sonic velocity and L the length of the pipe. By recording the time needed for 10 such reflections to occur, and averaging over several tests, we were able to estimate the actual sonic velocity to be

$$a = 2811 \, \text{feet/s} \quad = 857 \, \text{m/s}$$

Due to the relatively long pipe lengths, pressure loss due to pipe friction was found to be significant. Friction loss can be computed as

$$\Delta p = \lambda \frac{L}{D} \frac{\rho}{2} v^2. \tag{2}$$

Here λ is a friction coefficient (with 0.02 being a standard value), L is pipe length, D stands for pipe diameter, ρ is the density of the liquid and v is the average flow velocity in the pipe. Using this formula we found that the pressure loss at capacity was typically about 1% per foot of pipe and considerably less than that for lower flow rates. We have used this calculation to compute the 3% inlet line criterion mentioned in the Introduction. Because the pipe was mounted vertically, we also calculated hydrostatic pressure loss, but this was found to be almost negligible in comparison.

2.2. Typical time histories

During the measurements we observed three types of dynamics: either the valve was fully stable during the whole process; or it was found to be unstable during closing (i.e. during ramp down) and occasonally during opening also; or the valve was found to be fully unstable during the entire opening and closing cycle. sometimes also upon opening). Examples of each kind of behaviour are depicted in Fig. 2.

An example of a fully stable test is depicted in Fig. 2(a), (b). In all such tests, it was generally experienced that the valve opens in a modulated way. That is, with increasing tank pressure, the valve lift increases continuously up to 5-10% of full lift, and then jumps to an upper lift position. This jump is an example of a static instability (fold bifurcation) presumably due to a nontrivial effective area versus lift curve, as analyzed in Hős et al. (2014). Note from the inset to the lift plot that the valve lift is initially very gentle. During ramp down of the pressure, the valve closes through an initially
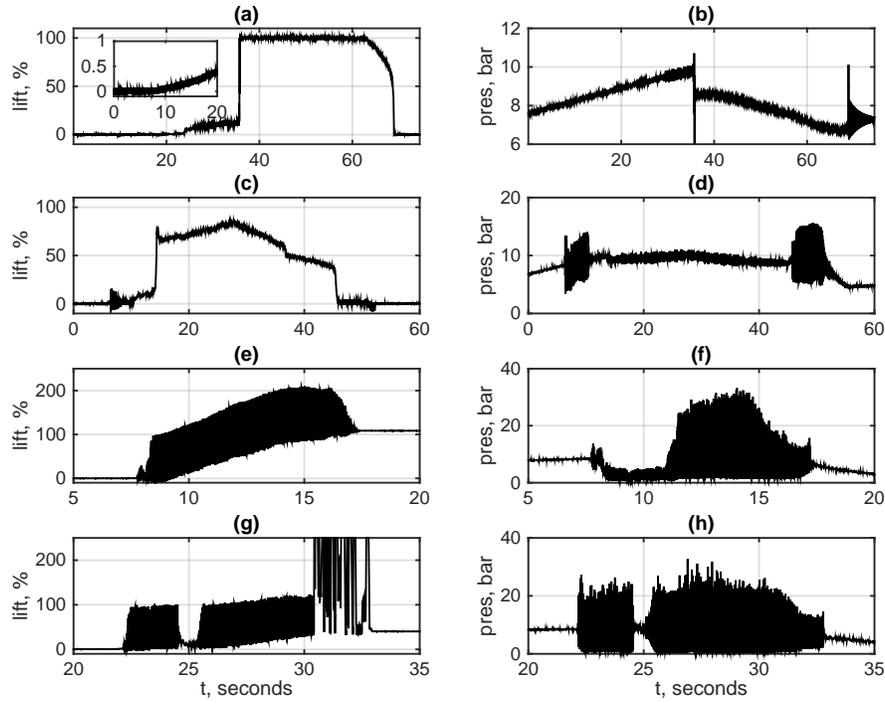
Figure 2: Plots of the valve lift (left), expressed as a percentage of full lift, and the pipe pressure at the valve inlet (right) for representative test runs on the 2J3 valve for different pipe lengths L and mass flow rates q (expressed as percentage of capacity flow rate). (a),(b) $L = 0$ and $q = 100\%$; the inset in (a) shows the onset of non-zero lift at around 10 seconds). (b),(c) $L = 4$ foot (1.22m), $Q = 85\%$. (e),(f) $L = 6$ foot (1.83m), $Q = 30\%$; (g), (h) $L = 6$ foot, $Q = 20\%$. Valve lift in (e) and (g) more than 100% indicates where the displacement sensor became detached due to the violence of the valve hitting its upper stop.

8

modulated phase followed by a sudden jump into a fully closed position. A particular contrast with the measurements in gas service presented in Hős et al. (2014) though is that, even in this stable opening case, once the flow builds up, significant pressure peaks can be observed whenever the valve lift jumps, in addition to pressure "noise" at the valve inlet even when the lift remains fairly static. Such pressure variations are typically of all stable runs, and were found to be equally well pronounced in the readings taken at pressure sensors PU, PL, yet the tank pressure measurement TK was relatively smooth (results not shown).

Fig. 2(c),(d) shows a relatively rare case where there is an instability upon opening that quickly stabilizes during the initially modulated phase before the dynamic jump to the upper equilibrium lift. This is matched by another brief instability as the valve closes. Much more common among the unstable cases is the example shown in Fig. 2(e),(f). Here, as soon as the instability occurs, it is particularly violent and almost immediately chatter ensues, in which the valve impacts with its seat (and also with its upper stop at 100% full lift). Unlike in gas service, in no case were we able to observed sustained valve flutter, that is rapid periodic valve motion without impacts.

Note how, even though for static lift the blow down for this valve was just 5%, for this unstable case, the tank pressure had to go well below the reseat pressure (perhaps by as much as 25%) to stop the chattering and close the valve again. In fact, during the initial chatter, the pressure in the pipe appears to drop, although the tank pressure continues to rise. This may be an artifact of the pressure measurement protocol during this violent motion. Later during the chatter phase, notice how the measured pressure in the pipe significantly exceeds the set pressure, by over 300%. These observations are typical of every time that chatter was seen. It would seem that these high pressure peaks are due to the well known phenomenon of water hammer (Wylie and Streeter (1993)) in hydraulic systems. That is, when the valve opens or closes quickly, it has to rapidly change the momentum of the fluid column inside the pipe. To quantify this effect, we suppose the valve closes in a time Δt and calculate the pressure force F that decelerates the fluid. If the valve closure is sufficiently slower than the timescale of reflected waves, $\Delta t \gg T_{\mathrm{pipe}}$ given by (1), then

$$F = A\Delta p = m\frac{dv}{dt} = \rho V\frac{dv}{dt} \approx \rho AL\frac{\Delta v}{\Delta t} \quad \rightarrow \quad (\Delta p)_{\mathrm{slow}} = \rho L\frac{\Delta v}{\Delta t}, \quad (3)$$

If the valve closing is particularly rapid though, one has to use the Joukowsky

equation, which gives

$$(\Delta p)_{\text{sudden}} = \rho a \Delta v, \tag{4}$$

Using (3) and (4) we can estimate the pressure amplitudes corresponding to different closure times. Taking the case of a 2J3 valve at capacity flow rate in a 2-inch diameter pipe we have $\Delta v = 40.9\,\text{feet/s} = 12.5\text{m/s}$ and an 8ft pipe the characteristic time of wave reflection is $T_{\text{pipe}} = 2L/a = 0.0058s$. Hence we can calculate the pressure peaks for different valve closure times, see Table 1. In the experiments, we were not able to resolve the precise timescale of valve closure to the accuracy required, but the values in the table offer a convincing explanation of why pressure fluctuations of the order of several hundred psi were recorded during valve chatter.

	$\Delta t \ll T_{\text{pipe}}$ =0.0058s	$\Delta t = 3T_{\text{pipe}}$ =0.0174s	$\Delta t = 10T_{\text{pipe}}$ =0.058s
Δp [bar]	105	17.6	5.27
Δp [psi]	1528	255	76.4

Table 1: Calculated water hammer pressure peaks for different valve closure times in the case of a 2J3 valve connected to an 8-foot pipe.

Fig. 2(g) and (h) show an example of measurement in which the valve is found to become immediately unstable upon opening. Curiously though in this case there is a short window of time (at around 25 seconds), in which the valve seems to stabilize, before quickly becoming unstable again. Given that the tank pressure and mean flow rate do not change significantly during this time interval, this would seem to be evidence that there is bistability between violent chattering motion and stable valve lift. We conjecture that this behaviour is due to the fact that this measurement is close to the stability boundary (in fact, just within the stability region) and, as will be confirmed later, the Hopf bifurcation marking the stability boundary is in fact *subcritical*, meaning that the stable equilibrium is surrounded by an unstable limit cycle. Transient effects can cause vibrations that go beyond the unstable boundary and jump into chatter. Similarly, transient perturbations to chatter can cause jumps into the stable equilibrium.

2.3. Stability charts

We can summarize the results of the tests in the form of stability charts. In each case we depict each measurement point according to two parameters
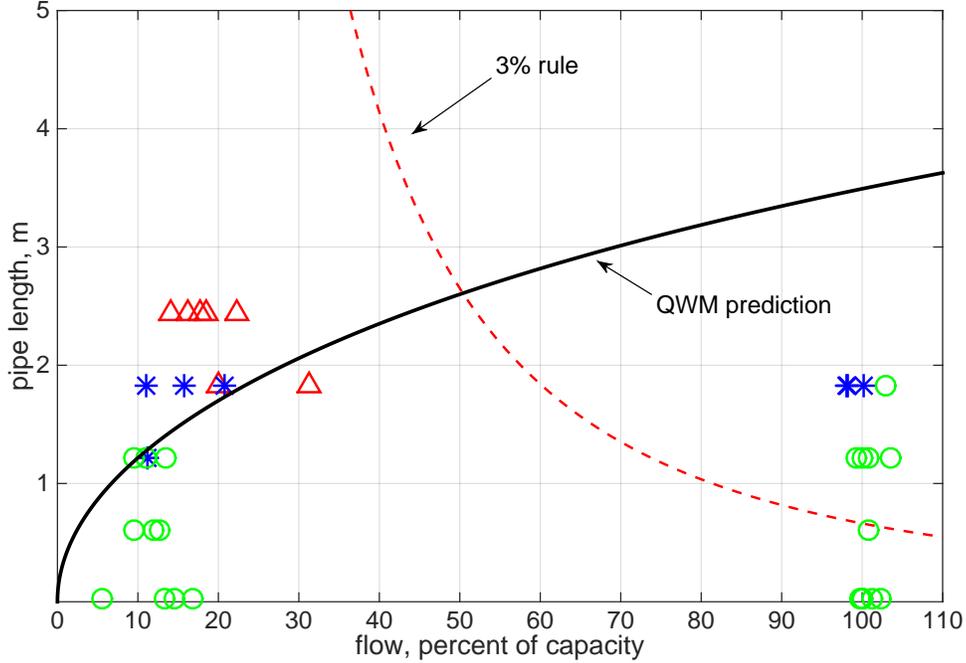
Figure 3: 2J3 test results. Different symbols represent the measurement points: (red, color online) triangles show test runs that were fully unstable, (blue) asterisks are unstable on closing, (green) circles are fully stable. Two theoretical predictions are presented for completeness, the (red) dashed line shows the critical pipe length corresponding to the 3% rule, and the (black) solid line is the analytical prediction for the quarter-wave instability (see text for details). In both cases, the stability criterion is that the measurements should lie beneath these curves.

of the test; the steady flow rate reached upon ramping up (given as a percentage of capacity) along the horizontal axis, and pipe length on the vertical axis.

Figure 3 depicts the results for the 2J3 valve. Also plot are two different analytical criteria that have been used to predict instability thresholds. The solid line depicts the analytical estimate of the quarter-wave model (QWM); see Sec. 3, specifically equation (15) below. The dashed line represents the '3% rule' that friction loss in the inlet pipe (calculated according to (2)) should be no more than 3% of the set pressure. Notice how the 3% rule has exactly the wrong trend. Many unstable points (for low flow rates in

particular) are beneath this curve. In contrast, the quarter-wave instability prediction provides a good explanation of the threshold of instability observed in the experiment, with a couple of exceptions.

The first exception is the fully unstable point at 30% capacity with a 6ft pipe. Note however, that this is case shown in Figure 2, which shows bistability and we already indicated could point to being just inside a stability threshold (see the discussion on subcriticality of the Hopf bifurcation in Sec. 4 below).

The other exception is the cluster of points that are depicted as being unstable on closing for a 6ft pipe at close to 100% capacity. Note that these cases were found to trigger instability only as the flow rate drops from its maximum. The flow rate at the point the instability occurs is hard to accurately measure, but in reality it will be significantly less than the capacity flow rate and so these points really represent flow rates that are significantly further to the left in the figure.

Figure 4 depicts results for the 1E2 valve. Again the results are consistent with the quarter-wave instability prediction and inconsistent with the 3% rule. Note that for a 12ft pipe, the vibrations were so violent that it was impossible to reach the capacity flow rate. This would be worrisome in practice as the desired pressure could not be relieved in this case.

Finally, looking at both Figs. 3 and 4 and comparing with the equivalent results for the same valves with nitrogen gas (Hős et al., 2014, Figs. 15 and 16), we find that the critical pipe length for instability is almost five times longer.

3. Mathematical modelling

We present here the necessary adaptations for dealing with liquids, to the gas-dynamic model in Hős et al. (2014). This leads to a simpler form of reduced model, as was first shown by Bazsó et al. (2015). It is useful here to present this model liquid model again, as we shall perform a different nondimensionalization in which flow rates are expressed as percentages of valve capacity. All physical constants are defined in Table 2, together with their values for the two valves tested.

The model considers the configuration shown in Fig. 5, with unknowns being the valve lift $x_v(t)$, reservoir pressure $p_r(t)$ and fluid velocity and pressure $v(s,t)$ $p(s,t)$, where $s = 0$ corresponds to the reservoir end of the pipe and $s = L$ to the valve end. The equations of motion can be written in the
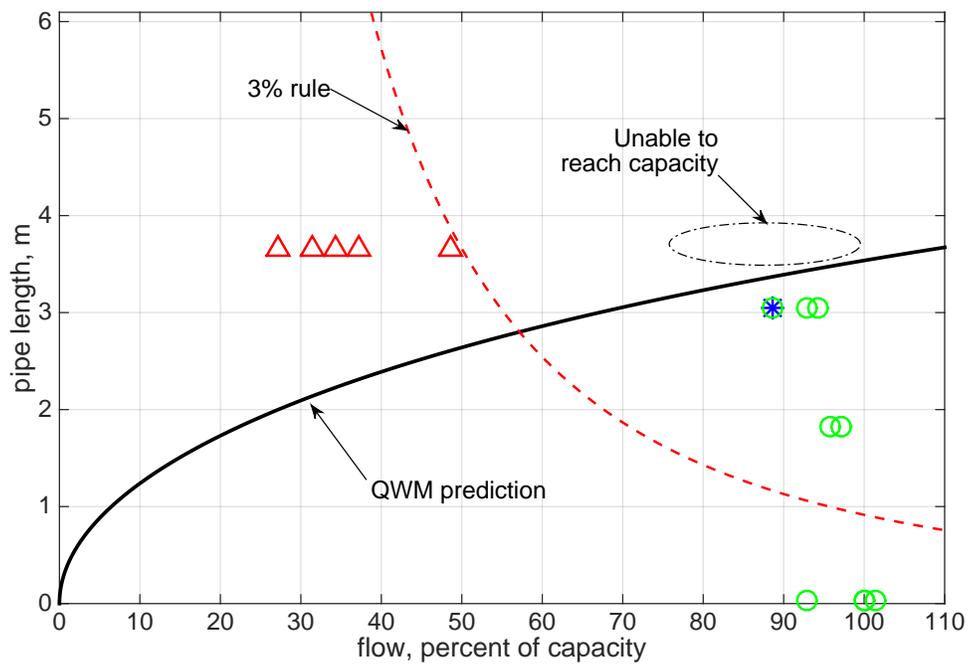
Figure 4: Similar to Fig. 3 but for the 1E2 valve test results. With the 12-foot pipe the oscillations were so severe that the capacity flow rate could not be reached.
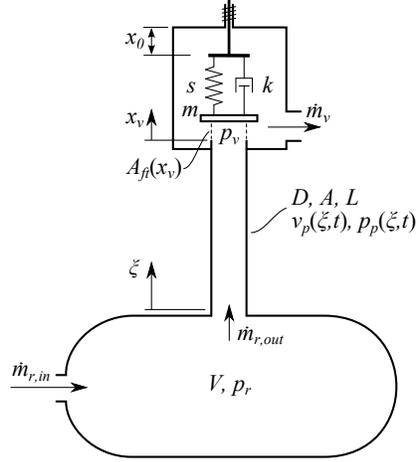
Figure 5: Definition sketch of the mathematical model developed in Hős et al. (2014)

Quantity	Symbol	1E2	2J3	Units
Mass flow rate	$\dot{m}_{r,in}$	0-3.8	0-23.4	kg/s
Pipe length	L	0-3	0-3	m
Pipe diameter (nom. inner)	D	0.0266	0.0525	m
Effective pressure diameter	D_{eff}	0.0161	0.0444	m
Seat diameter	D_{seat}	0.0161	0.0407	m
Reservoir volume	V	10.6	10.6	m^3
Total effective moving mass	m	0.4392	1.43	kg
Spring constant	s_v	1.69	4.79	kN/m
Damping coefficient	% of k_{crit}	0%	0%	-
Set pressure	p_{set}	6.9	8.27	bar
Spring pre-compression	x_p	9.2	23	mm
Coefficient of discharge	C_d	0.32	0.36	-
Coefficient of restitution	r	0.8	0.8	-
Maximum lift	x_{max}	5.2	12	mm
Sonic velocity	a	890	890	m/s
Ambient pressure	p_0	1	1	bar
friction factor	f	0.02	0.02	-

Table 2: Default parameter values used for each of the two valves.

14

form

$$m\ddot{x}_v + k\dot{x}_v + s_v(x_p + x_v) = (p_v - p_b)A_{\text{eff}}(x_v), \quad \text{for } x_v > 0 \qquad (5)$$

$$\dot{p}_r = \frac{a^2}{V}\left(\dot{m}_{\text{in}} - \dot{m}_{\text{out}}\right), \qquad (6)$$

$$0 = \frac{\partial p}{\partial t} + \rho a^2 \frac{\partial v}{\partial s} + v\frac{\partial p}{\partial s}, \qquad (7)$$

$$0 = \frac{\partial v}{\partial t} + v\frac{\partial v}{\partial s} + \frac{1}{\rho}\frac{\partial p}{\partial s} - \lambda\frac{1}{2D_{\text{pipe}}}v^2, \qquad (8)$$

where m is the mass of the moving parts (valve body plus 1/3 spring mass), k is viscous damping, x_p stands for spring precompression, $p_v(t) = p(L,t)$ is the pipe pressure at the valve end and p_b is the backpressure. $A_{\text{eff}} = F_{fluid}/(p_v - p_b)$ is the valve's effective area as a function of lift, which is typically empirically determined from valve measurements. In equation (6) p_r is the reservoir pressure, a stands for sonic velocity, V is the volume of the reservoir, $\dot{m}_{\text{in}}$ is the *constant* mass flow rate entering the reservoir and $\dot{m}_{\text{out}}$ is that leaving (and entering the pipe), given by

$$\dot{m}_{\text{out}} = A_{\text{pipe}}\rho v(0,t).$$

At the reservoir end of the pipe, we assume ideal inflow from the reservoir which gives

$$p_r(t) = p(0,t) + \frac{\rho}{2}\left(v(0,t)\right)^2.$$

At the valve end of the pipe, the continuity equation implies

$$v(L,t)A_{\text{pipe}}\rho = C_d A_{\text{ft}} x_v \sqrt{\frac{\rho}{2}\left(p(L,t) - p_b\right)}. \qquad (9)$$

A Newton restitution law is assumed at $x_v = 0$ with $\dot{x}_v < 0$: $\dot{x}_v^+ = -r\dot{x}_v^-$.

Note how the equations are simpler than the gas case, cf. (Hős et al., 2014, eq. (11)), because we are able to assume linearized (slightly compressible) equations of for the pressure $p(s,t)$ and velocity $v(s,t)$. Also, we do not have to assume choked flow upon discharge.

3.1. Nondimensionalization

In order to simulate and analyze the coupled system of equations (5)–(9) it is helpful to first introduce a dimensionless version. See Table 3 which gives the reference pressure, displacement, frequency, velocity and mass flow rate, together with various natural dimensionless parameters that appear in the equations. Note that we assume there to be no back-pressure so that reference pressure is ambient. The reference mass flow rate $\dot{m}_{cap}$ is the capacity of the valve, that is the mass flow rate at pressure 10% above set pressure and full lift.

Note that with this rescaling, the main driving parameter q measures the mass flow rate entering the reservoir as a fraction of the valve capacity. Then an additional parameter μ arising during the nondimensionalization represents a ratio of two mass flow rates

$$\mu = \frac{A_{\text{pipe}}\rho\omega x_{\text{ref}}}{\dot{m}_{\text{cap}}}, \tag{10}$$

and

$$\sigma = \frac{c_2 x_{\text{ref}}\sqrt{\rho p_{\text{ref}}}}{A_{\text{pipe}}\rho x_{\text{ref}}\omega_v}. \tag{11}$$

parameterizes the ratio between valve and fluid velocity scales.

We now define dimensionless variables via $s = x_{\text{ref}}\xi$, $t = \tau/\omega_v$, letting $' = \frac{d}{d\tau}$, and $x_v = x_{\text{ref}}y_1$, $\dot{x}_v = \omega_v x_{\text{ref}}y_2$, $p_r = p_{\text{ref}}y_3$, $p(s,t) = p_{\text{ref}}\tilde{p}(\xi,\tau)$ and $v(s,t) = \omega_v x_{\text{ref}}v(\xi,\tau)$ and rewrite system (5), (6), (7) and (8). The meaning and definition of each of dimensionless parameters appearing in these equations are given in Table 3. An additional parameter appearing is Λ is a length scale that measures the importance of the nonlinear, convective terms. It can expressed as

$$\Lambda = \frac{x_{\text{ref}}}{L} := \frac{\nu\alpha}{\gamma}. \tag{12}$$

Here we find a key difference between gas flows and liquid flows: in Hős et al. (2015), we found that Λ is related to Mach number and can become $O(1)$ close to capacity flow rates. Here however, we find that from Table 3 that $\Lambda = O(10^{-2})$ and so is largely unimportant, compared with fluid-structure interaction nonlinearities.

To simulate the above equations, we discretize using the method of characteristics, see Wylie and Streeter (1993) for details. Computations are carried out in dimensionless units, but for comparison with experimental results, all results are presented using dimensional variables.

Quantity	Symbol	Definition	2J3	1E2
Reference pressure, bar	p_{ref}	$p_b = p_0$	1	1
Reference displacement, mm	x_{ref}	$\frac{A_{\text{eff}} p_{\text{ref}}}{s}$	1.78	3.29
Reference frequency, rad/s	ω_v	$\sqrt{s/m}$	201.3	180.5
Capacity mass flow rate, kg/s	$\dot{m}_{\text{cap}}$	see text	3.8	23
Mass flow rate ratio, -	μ	eq. (10)	0.0538	0.05459
Driving mass flow-rate, -	q	$\frac{\dot{m}_{\text{in}}}{\dot{m}_{\text{cap}}}$	0-1	0-1
Spring pre-compression, -	δ	$\frac{s_v x_p}{A_{\text{seat}} p_b}$	5.17	6.9803
Pipe length parameter, -	γ	$\frac{L\omega}{a}$	varied	varied
Reservoir-size parameter, -	β	$\frac{a^2}{V} \frac{\dot{m}_{\text{cap}}}{p_{\text{ref}}\omega}$	varied	varied
Valve damping, -	κ	$\kappa = \frac{k}{m}\sqrt{\frac{m}{s}}$	0	0
Velocity-to-mass flow rate par., -	σ	eq. (11)	2.352	1.668
Ambient pressure, -	ν	$\frac{p_0}{\rho a^2}$	0.000126	0.0027
Velocity-to-sonic velocity par., -	α	$\frac{\rho A_{\text{eff}} a}{m\omega} = \frac{1}{\nu}\frac{v_{\text{ref}}}{a}$	3.186	5.2917
Friction factor, -	ϕ	$f\frac{x_{\text{ref}}}{2D_{\text{pipe}}}$	0.00064	0.00063

Table 3: Reference scales and dimensionless parameters together with their values for the 2J3 data in Table 2.

3.2. Model reduction and quarter-wave instability analytical prediction

In Hős et al. (2014) we performed a spectral decomposition of the equations of motion in the case of gas, by expanding the pipe pressure and velocity into a finite number N of acoustic modes in the pipe. We showed that instabilities are always well ordered, in that the first instability to be encountered upon increasing pipe length for a fixed flow rate is always due to a coupled instability between the valve motion and the first acoustic mode, the so-called quarter-wave mode, with (dimensional) wavelength 4L. Thus to predict instability, we can assume that all acoustic energy is contained in this mode. Setting $\Lambda = 0$ we thus assume

$$\tilde{p}(\xi, \tau) = y_3(\tau) + B(\tau) \sin \left(\frac{\pi}{2} \xi \right) \tag{13}$$

$$\tilde{v}(\xi, \tau) = \sigma y_1 \sqrt{y_3(\tau) + B(\tau)} + C(\tau) \cos \left(\frac{\pi}{2} \xi \right) \tag{14}$$

and applying a 1-point collocation technique to obtain closed form equations for B' and C' (see Bazsó et al. (2015) for details). Thus the instability can be predicted by just solving the five ordinary differential equations for $y(t)$, $y'(t)$, $p(t)$, $B(t)$ and $C(t)$, which is known as the quarter-wave model for liquids. Note that this is a simplification of the quarter-wave model for gas presented in Hős et al. (2015) because the nonlinear convection effects and inlet pressure loss terms can be ignored.

In fact, in Hős et al. (2015) it was further shown that by analyzing the quarter-wave model without inlet pressure loss and convection terms, then in certain asymptotic limits an analytic expression can be derived for the quarter-wave instability. The asymptotic limits in question are

$$\beta\mu \ll 1, \quad \frac{\alpha}{\gamma}, \quad \text{and} \quad q \ll \frac{1}{\sigma\mu},$$

which can readily be seen to be satisfied in the liquid case too, (see Table 3). Thus the analytical estimate derived for the quarter-wave instability in gas service is still valid, namely (Hős et al., 2015, Eq. (48))

$$\text{instability for} \quad q < 2\frac{(1+\delta)^{3/2}}{\omega_1^2 - 1}\mu\sigma, \tag{15}$$

where $\omega_1 = \frac{\pi}{2\gamma}$ is the dimensionless quarter-wave frequency. This formula leads to a square root expression for the critical pipe length as a function of flow rate for sufficiently small flow rates, and is the formula plotted as a solid curve in the Figs. 3 and 4.

18

3.3. Analytical prediction of a Helmholtz-like instability

Our simulations have shown that there can be another instability for very short pipe lengths that was not apparent for pipes in gas service. This is a Helmholtz-like instability where the fluid in the pipe undergoes plug-like motion *in phase* with the valve. In contrast to the quarter-wave instability, we have found the Helmholtz-like instability to occur if the inlet pipe is *short enough*. In theory this instability is always present in any form of fluid, but for gas flow with realistic tank volumes it would only occur for pipe lengths of less than a thousandth of an inch, which is clearly both practically unobservable and also well outside the range of validity of any model.

To show how this form of instability can arise we start with the quarter-wave model, which ignoring valve damping, friction and convection effects in (Hős et al., 2015, Eqs. (34),(35)) can be written in dimensionless form as

$$y'' = (p + B - 1) - (\delta + y) - ky', \tag{16}$$

$$p' = \beta \left[q - \mu(\sigma y \sqrt{p + B} + C) \right], \tag{17}$$

$$B' = \frac{\pi}{2} \frac{\alpha}{\gamma} C - \sqrt{2} p', \tag{18}$$

$$C' = -\frac{\pi}{2} \frac{1}{\alpha \gamma} B - \sqrt{2} \sigma \frac{d}{d\tau} y \sqrt{p + B}. \tag{19}$$

Furthermore, we change variables such that the equilibrium $(y, p, B, C) = (y_0, p_0, 0, 0)$ moves to the origin. That is, we set

$$y = y_0 + Y, \qquad p = p_0 + P,$$

so that the valve equation (16) reads

$$Y'' = (P + B) - Y.$$

We notice that if the term $(P + B)$ is small then this can be regarded as a form of nonlinear damping (note (17) that P' contains a term proportional to Y, so that $P(t)$ will involve components that are $\pm\pi/2$ out of phase with Y). Moreover, if this term were to precisely vanish, then we would have a completely undamped oscillator. Thus if we smoothly vary a parameter through a value where $(P + B)$ vanishes, in general we will have a transition from positive (dissipative) damping to negative (excitatory) damping. Thus we can view the vanishing of $(P + B)$ as representing a point of instability

19

of the valve motion. In fact, numerical simulation has shown that negative damping occurs for shorter pipes, whereas there is dissipation of the valve motion via this process for longer pipes. Hence we can seek an instability threshold in which

$$P(t) \equiv -B(t), \qquad \text{for all time.} \tag{20}$$

which would lead to an instability upon reducing the pipe length.

Suppose parameter values can be found for which (20) is satisfied, then the valve equation becomes completely linear $Y'' = -Y$ which has solution $Y(t) = A\cos(t + \psi)$ for an arbitrary amplitude A and phase ψ. We also note that a remarkable thing happens to the other equations, they also become completely linear:

$$P' = -\beta\mu(\sigma Y\sqrt{p_0} + C), \tag{21}$$

$$B' = \frac{\pi}{2}\frac{\alpha}{\gamma}C - \sqrt{2}P', \tag{22}$$

$$C' = -\frac{\pi}{2}\frac{1}{\alpha\gamma}B - \sqrt{2}\sigma\sqrt{p_0}Y'. \tag{23}$$

Hence we shall seek a coupled linear solution in which all variables are all oscillating at the same (valve natural) frequency. That is,

$$P(t) = -B(t) \sim \cos(t), \quad Y(t) \sim \cos(t + \psi), \quad C(t) \sim \cos(t + \phi), \tag{24}$$

for some unknown phases ψ and ϕ.

It remains to find parameter conditions in which the linear equations (21)–(24) are consistent. To find such conditions we first set $B' = -P'$ from (21) and (22) we get two different expressions for B' which must be set to be equal, leading to the condition

$$a_{11}Y + a_{12}C = 0, \quad \text{where } a_{11} = \beta\mu\sigma\sqrt{p_0}, \quad a_{12} = \left(\beta\mu + \frac{\alpha\pi}{2\gamma(\sqrt{2}-1)}\right) \tag{25}$$

Similarly we can differentiate (23) with respect to τ, use $C'' = -C$ and $Y'' = -Y$ from (24) and eliminate B' using (21) (after setting $P' = -B'$). The resulting equation can again be written as a linear condition between C and Y:

$$a_{21}Y + a_{22}C = 0, \quad \text{where } a_{21} = \sigma\sqrt{p_0}\left(\sqrt{2} - \frac{\beta\mu\pi}{2\alpha\gamma}\right), \quad a_{22} = 1 + \frac{\beta\mu\pi}{2\alpha\gamma}. \tag{26}$$

For (25) and (26) to be consistent, we must have that

$$a_{11}a_{22} - a_{12}a_{21} = 0, \tag{27}$$

which can be expressed as a cubic equation in $1/\gamma$ with a single positive root $(1/\gamma) = (1/\gamma_c)$. Then instability would occur for $\gamma < \gamma_c$.

In the case that $\alpha/(\beta\mu) \gg 1$ (according to table 2, this ratio is $O(10^2)$) then we can write the solution to (27) in the form

$$\frac{\beta\mu\pi}{2\alpha\gamma_c} = \sqrt{2} + \mathcal{O}([\beta\mu/\alpha]^2).$$

Using this value for γ_c we find the criterion for instability to be

$$\gamma < \gamma_c = \frac{\pi\beta\mu}{2\sqrt{2}\alpha} + \mathcal{O}((\mu\beta/\alpha)^3). \tag{28}$$

In summary, we have an instability for dimensionless pipe lengths γ less than the critical length given by (28), *independent of the mass flow rate q*. The form of the instability is such that the motion is at the valve's natural frequency (angular frequency 1 in dimensionless units) and the pipe velocity, tank pressure, pipe pressure and pipe velocity are all synchronous, with the tank pressure and pipe pressure variations being precisely out of phase; $B = -P$. Note from the form of (28) that this condition can be written in terms of the Helmholtz resonance condition

$$\omega_v^2 = \frac{\pi}{2\sqrt{2}}\omega_H^2$$

where ω_H is the *Helmholtz resonance frequency* of the tank and pipe.

4. Simulation results and parameter trends

Extensive runs of the full simulation model were undertaken under both steady inlet conditions and ramped pressure variation as in the experiments. The simulation model was found to agree well with experimental results in all cases. We show a summary of the steady results for the 2J3 valve in Fig. 6 for a grid of values of flow rate and pipe length. Similar results were found for the 1E2. In the figure we have indicated by a green circle the parameter values for which stable operation was found, and by a red cross those values that were found to be unstable. In almost all cases where instability was
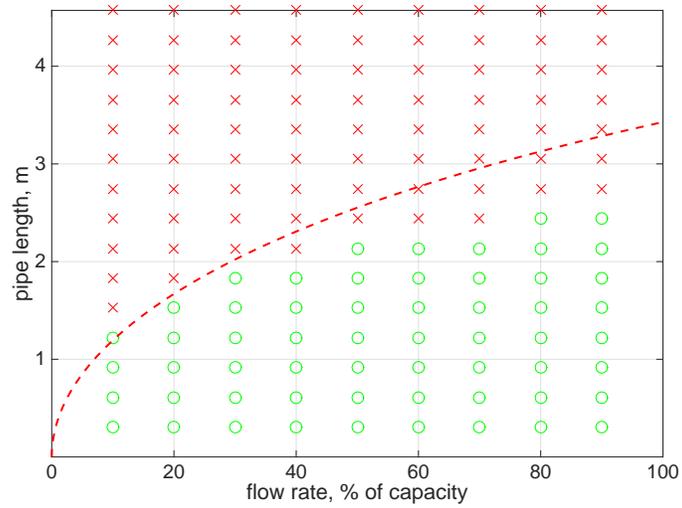
21

Figure 6: Summary of the computation results for the 2J3 valve with a large reservoir, $V = 375\,\text{ft}^3$, $\beta = 0.097$. The dashed line depicts the analytical estimate (15) of the quarter-wave stability boundary. Crosses (red - color online) depict simulations for which the valve was found to be unstable, and (green) circles depict points for which the valve was computed to be stable.

found, the valve was found to quickly transition into chatter after very few cycles. We have also plot the stability condition (15), which is the same curve as the solid black line in the experimental results of Fig. 3.

Furthermore, we were able to run the reduced-order model to perform precise computation of the quarter-wave instability boundary and to continue this as a curve in pipe length versus flow rate. It was found to differ from the analytic approximation by only a few percent. Moreover, the Hopf bifurcation represented by this instability curve was found to be sub-critical for all but the very lowest flow rates. This would seem to explain why a stable flutter limit cycle was virtually never observed, with the valve jumping straight into chatter instead.

set pressure	spring rate	δ	α	σ	μ	β	L_{ref}
psi	N/mm						m
100	84.6	4.90	6.142	1.817	0.0585	0.0957	4.47
250	236.2	11.36	3.019	0.893	0.0189	0.0716	2.20
500	483.7	22.72	2.110	0.624	0.0093	0.0707	1.54
750	702.4	34.08	1.751	0.518	0.0063	0.0719	1.27
1000	939.7	45.44	1.514	0.448	0.0047	0.0718	1.10

Table 4: Dimensionless parameters for several set pressures for the 2J3 valve.

Figure 7 shows the trend of the quarter-wave instability upon varying set pressure (using stiffer springs) – see Table 4 for how we calculated the set pressure based on the dimensionless parameters. We find that the liquid service valve behaves in the same way as the gas valve did in Hős et al. (2015). That is, the higher the set pressure, the lower the critical pipe length for stability. This trend was also found in experimental tests (results not shown). We also depict in figure 7 the critical pipe lengths computed according to the 3% rule. It is important to note that the 3% rule predicts that the critical pipe length should *increase* with set pressure (because we take the 3% of a higher set pressure) whereas the real tendency is just the opposite.

Finally, Fig. 8 shows the result of a similar set of computations as in Fig. 6 but with a reservoir volume that is significantly smaller than that used in the experiments. Note here that the quarter-wave stability curve is largely unchanged, but that the Helmholtz-like instability is now predicted to occur up to a significant pipe length. This prediction is indeed borne out
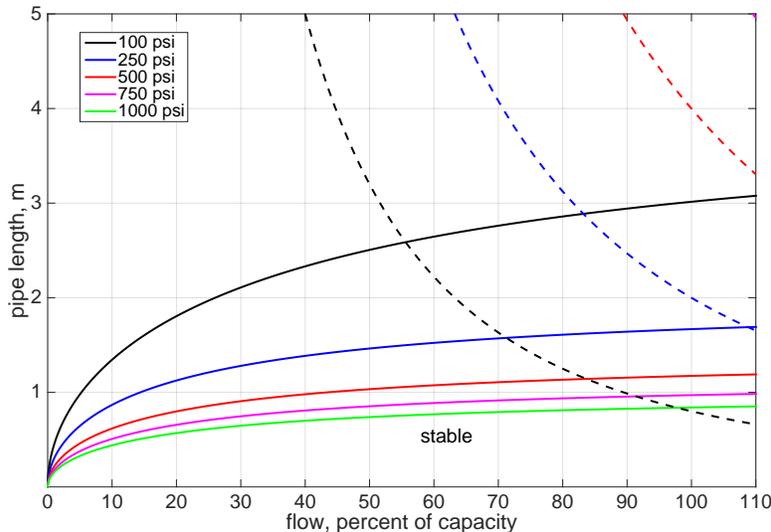
Figure 7: Effect of set pressure, computed by means of (15). Also plot for comparison as dashed lines are the equivalent curves corresponding to the 3% rule.

by the simulations; there is an additional region of instability for pipe lengths beneath that predicted by the formula (28).

Further parameter studies indicate that if we include significant valve damping $\kappa > 0$, then we find that the Helmholtz-like threshold curves downwards in the flow-rate versus pipe length plane (q versus γ), eventually hitting $\gamma = 0$. Additionally, the quarter-wave instability begins to curve upwards significantly for moderate q values. Thus the two-parameter bifurcation diagram becomes the one computed in (Bazsó et al., 2014, Fig. 8), in which the zero-pipe-length case is once again stable for sufficiently large q. That study was based on parameter values for a laboratory valve that had very different characteristics than the commercial standard valves under investigation in this paper.

5. Conclusion

In summary, this paper has extended the earlier experimental and simulation results to cover the case of valves in liquid service. Use of the reduced-order quarter-wave model derived in earlier work has enabled us to perform
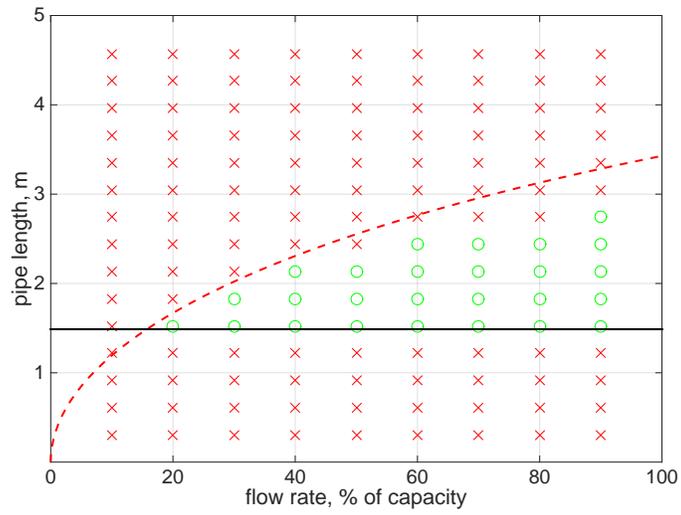
Figure 8: Summary of the computation results for the 2J3 valve with a small reservoir, $V = 1.25\,\mathrm{ft}^3$, $\beta = 29.23$. The dashed line depicts the analytical estimate (15) of the quarter-wave stability boundary, the dash-dot line depicts the critical pipe length corresponding to the Helmholtz instability, given by (28). Crosses (red - color online) depict simulations for which the valve was found to be unstable, and (green) circles depict points for which the valve was computed to be stable.

25

parameter studies showing dependence of instabilities on valve and inlet properties and to test the validity of the analytical formulae. We find both similarities and differences from the gas service case.

First, we find a similar trend in the fundamental instability criterion, namely that there is an approximately quadratic relationship between the critical mass flow rate and inlet pipe length. Operation at points above this curve will lead to instability. This curve is derived from an analytical approximation to the condition for there to be a so-called quarter-wave instability, which is a Hopf bifurcation caused by the interaction between the valve's dynamics and the fundamental acoustic mode in the pipe. In one sense we find that liquid service valves are more stable; for similar valve parameters, the critical pipe length for stability is generally almost five times longer for the liquid used (water) than it was for the gas (nitrogen).

However, when the quarter-wave instability does occur it is far more violent than it is for gasses. This we have found to be because the Hopf bifurcation is *subcritical*. This means that instead undergoing stable limit cycle motion (valve flutter), the post-instability motion will jump quickly to fully chattering solutions in which the valve repeatedly impacts with its seat. This chattering motion will lead to large pressure variations in the pipe due to water hammer effects each time the valve impacts with its seat. Also, subcriticality means that the predicted instability threshold is a pessimistic bound because transient jumps in the sub-threshold region can also trigger instability, with the size of the required transient shrinking to zero as the threshold is approached.

Experimentally, we found cases where instability was sufficiently extreme that transient pressures in the pipe could reach up to five times that of the set pressure. We also found cases where upon ramping up the pressure, it was not possible to reach mean mass flow rates that are sufficient to relieve the overpressure. Thus the avoidance of instability for direct-spring operated pressure relief valves in liquid service should be of critical importance in practice.

Additionally for liquids, we found the decreased compressibility can cause another instability to become significant. This is a Helmholtz-like instability where the valve and tank pressure move in unison. Unlike the quarter-wave, this instability occurs for inlet pipes that are too short, rather than too long. It can also be predicted by an analytical formula, but is only likely to be significant in practice if there is a small reservoir.

26

Acknowledgements

References

Bazsó, C., Champneys, A., Hős, C., 2014. Bifurcation analysis of a simplified model or a pressure relief valve attached to a pipe. SIAM Journal on Applied Dynamical Systems 13, 704–721.

Bazsó, C., Champneys, A., Hős, C., 2015. Model reduction of a direct spring-loaded pressure relief valve with upstream pipe. IMA J. Appl. Math. 80, 1009–1024.

Bazsó, C., Hős, C., 2012. A CFD study on the stability of a hydraulic pressure relief valve, in: Proceedings of CMFF12, pp. 428–434.

Beune, A., Kuerten, J., van Heumen, M., 2012. CFD analysis with fluid-structure interaction of opening high-pressure safety valves. Computers and Fluids 64, 108–116.

Dossena, V., Marinoni, F., Bassi, F., Franchina, N., Savini, M., 2013. Numerical and experimental investigation on the performance of safety valves operating with different gases. International Journal of Pressure Vessels and Piping 104, 21–29.

Erdődi, I., Hős, C., . CFD simulation on the dynamics of a direct spring operated pressure relief valve. Proceedings of CMFF 15, Budapest.

Frommann, O., Friedel, L., 1998. Analysis of safety relief valve chatter induced by pressure waves in gas flow. Journal of Loss Prevention in the Process Industries 11, 279–290.

Hős, C., Champneys, A., 2012. Grazing bifurcations and chatter in a pressure relief valve model. Physica D: Nonlinear Phenomena 241, 2068–2076. doi:10.1016/j.physd.2011.05.013.

Hős, C., Champneys, A., Paul, K., McNeely, M., 2014. Dynamic behaviour of direct spring loaded pressure relief valves in gas service: model development, measurements and instability mechanisms. J. Loss Prevention Process Industries 31, 70–81.

Hős, C., Champneys, A., Paul, K., McNeely, M., 2015. Dynamic behaviour of direct spring loaded pressure relief valves in gas service: Ii reduced order modelling. Journal of Loss Prevention in the Process Industries 36, 1–12.

Licsko, G., Champneys, A., Hős, C., 2009. Nonlinear analysis of a single stage pressure relief valve. Int. J. Appl. Math 39, 12–26.

Moussou, P., Gibert, R., Brasseur, G., Teygeman, C., Ferrari, J., Rit, J., 2010. Instability of Pressure Relief Valves in Water Pipes. Journal of Pressure Vessel Technology 132, 041308.

Qian, J.Y., Wei, L., Jin, Z.J., Wang, J.K., Zhang, H., Lu, A., 2014. CFD analysis on the dynamic flow characteristics of the pilot-control globe valve. Energy Conversion and Management 87, 220–226.

Song, X., Cui, L., Cao, M., Cao, W., Park, Y., Dempster, W., 2014. A CFD analysis of the dynamics of a direct-operated safety relief valve mounted on a pressure vessel. Energy Conversion and Management 81, 407–419.

Song, X., Park, Y., Park, J., 2013. Blowdown prediction of a conventional pressure relief valve with a simplified dynamic model. Mathematical and Computer Modelling 57, 279–288.

Song, X., Wang, L., Park, Y., 2010. Transient analysis of a spring-loaded pressure safety valve using computational fluid dynamics (CFD). Journal of Pressure Vessel Technology 132.

Viel, A., Imagine, L., 2011. Strong coupling of modelica system-level models with detailed CFD models for transient simulation of hydraulic components in their surrounding environment, in: Proceedings of the 8th International Modelica Conference, pp. 256–265.

Wu, D., Li, S., Wu, P., 2015. CFD simulation of flow-pressure characteristics of a pressure control valve for automotive fuel supply system. Energy Conversion and Management 101, 658–665.

Wylie, E., Streeter, V., 1993. Fluid transients in systems. Printice Hall, New Jersey.